



3D-printable supramolecular hydrogels with shear-thinning property: fabricating strength tunable bioink via dual crosslinking

Tian Hu^{a,b,d,1}, Xiaoliang Cui^{c,1}, Meng Zhu^c, Man Wu^c, Ye Tian^c, Bin Yao^{a,b}, Wei Song^{a,b}, Zhongwei Niu^{c,e,2,***}, Sha Huang^{a,b,2,**}, Xiaobing Fu^{a,b,2,*}

^a Research Center for Tissue Repair and Regeneration Affiliated to the Medical Innovation Research Department, PLA General Hospital and PLA Medical College, 28 Fu Xing Road, Beijing, 100853, PR China

^b PLA Key Laboratory of Tissue Repair and Regenerative Medicine and Beijing Key Research Laboratory of Skin Injury, Repair and Regeneration, Research Unit of Trauma Care, Tissue Repair and Regeneration, Chinese Academy of Medical Sciences, 2019RU051, 51 Fu Cheng Road, Beijing, 100048, PR China

^c Key Laboratory of Photochemical Conversion and Optoelectronic Materials, Technical Institute of Physics and Chemistry, Chinese Academy of Sciences, Beijing, 100190, China

^d Chinese Academy of Medical Sciences (CAMS) Oxford Institute, Nuffield Department of Medicine, University of Oxford, Oxford OX3 9DS, UK

^e School of Future Technology, University of Chinese Academy of Sciences, Beijing, 100049, PR China

ARTICLE INFO

Keywords:

Supramolecular hydrogel
Bioink
Tunable strength
3D bioprinting

ABSTRACT

3-dimensional (3D) bioprinting technology provides promising strategy in the fabrication of artificial tissues and organs. As the fundamental element in bioprinting process, preparation of bioink with ideal mechanical properties without sacrifice of biocompatibility is a great challenge. In this study, a supramolecular hydrogel-based bioink is prepared by polyethylene glycol (PEG) grafted chitosan, α -cyclodextrin (α -CD) and gelatin. It has a primary crosslinking structure through the aggregation of the pseudo-polyrotaxane-like side chains, which are formed from the host-guest interactions between α -CD and PEG side chain. Apparent viscosity measurement shows the shear-thinning property of this bioink, which might be due to the reversibility of the physical crosslinking. Moreover, with β -glycerophosphate at different concentrations as the secondary crosslinking agent, the printed constructs demonstrate different Young's modulus ($p < 0.001$). They could also maintain the Young's modulus in cell culture condition for at least 21 days ($p < 0.05$). By co-culturing each component with fibroblasts, CCK-8 assay demonstrate cellular viability is higher than 80%. After bioprinting and culturing, immunofluorescence staining with quantification indicate the expression of Ki-67, Paxillin, and N-cadherin is higher in day 14 than those in day 3 ($p < 0.05$). Oil red O and Nissl body specific staining reflect strength tunable bioink may have impact on the cell fate of mesenchymal stem cells ($p < 0.05$). This work might provide new idea for advanced bioink in the application of re-establishing complicated tissues and organs.

1. Introduction

Three-dimensional (3D) bioprinting provides brand-new avenue for constructing artificial tissues and organs, especially those with complex components and hierarchical structures [1,2]. Bioink consists of biomaterials and cells, which is of irreplaceable importance in the process

of bioprinting. An ideal bioink requires good printability, mechanical properties [3] and biocompatibility to provide cell-friendly environment [4,5]. Good printability could guarantee the process of bioprinting, as well as yield the designed structure and shape of bioprinted construct. Mechanical properties are especially crucial for bioprinted construct to maintain the morphology after the bioprinting process. As

Peer review under responsibility of KeAi Communications Co., Ltd.

* Corresponding author. Research Center for Tissue Repair and Regeneration Affiliated to the Medical Innovation Research Department, PLA General Hospital and PLA Medical College, 28 Fu Xing Road, Beijing, 100853, PR China.

** Corresponding author. Research Center for Tissue Repair and Regeneration Affiliated to the Medical Innovation Research Department, PLA General Hospital and PLA Medical College, 28 Fu Xing Road, Beijing, 100853, PR China.

*** Corresponding author. Key Laboratory of Photochemical Conversion and Optoelectronic Materials, Technical Institute of Physics and Chemistry, Chinese Academy of Sciences, No.29 Zhongguancun East Road, Haidian District, Beijing, PR China.

E-mail addresses: niu@mail.ipc.ac.cn (Z. Niu), stellarahuang@sina.com (S. Huang), fuxiaobing@vip.sina.com (X. Fu).

¹ Tian Hu and Xiaoliang Cui contributed equally to this work.

² Authors to whom any correspondence should be addressed.

<https://doi.org/10.1016/j.bioactmat.2020.06.001>

Received 27 March 2020; Received in revised form 19 May 2020; Accepted 3 June 2020

2452-199X/© 2020 Production and hosting by Elsevier B.V. on behalf of KeAi Communications Co., Ltd. This is an open access article under the CC BY-NC-ND license (<http://creativecommons.org/licenses/by-nc-nd/4.0/>).

cells in the bioink need to be cultured in certain conditions, reasonable mechanical strength would not only help bioprinted constructs to maintain the structure, but also provide mechanotransduction signal to cells inside. Biocompatibility refers to good cellular behaviours when they are cultured with biomaterials, which include cell viability, proliferation, spreading, adhesion, migration, and so on.

A main challenge for bioink is to balance those conditions to largest extent. Most biomaterials with good mechanical properties usually suffer from poor cell friendliness, or vice versa. Hydrogels, which are highly hydrated 3D crosslinked polymers, become a typical category of component for bioink owing to their good biocompatibility, high water content and highly controllable 3D structure [6,7]. It could form an extracellular matrix-like structure to provide cells a mechanically supportive microenvironment and a spatial activity, which is advantageous for cell spreading, migration, interactions and differentiation [8]. In order to solve the problem, researchers in this area have investigated and invented numerous sorts of biomaterials that could meet different needs. Shear-thinning and long-time maintenance feature are required for printable hydrogels [9]. Polyrotaxanes (PRs) or pseudo-polyrotaxanes (PPRs), which have a “molecular necklace” structure, have been widely exploited in the field of molecular machines, energy storage and biomedicine [10,11]. PR or PPR structure is mainly resulted from the inclusion complexation between cyclodextrins (CDs) and polymers through host-guest interactions. The aggregation of the PR-like side chain may realize the formation of a supramolecular hydrogel, and the reversibility of this physical crosslinking provides it injectable shear-shinning property [12]. This supramolecular hydrogel cross-linked by weak physical bonding alone does not satisfy the mechanical requirement of bioink for a long-time shape maintenance. However, secondary crosslinking after bioprinting can solve this problem [13,14].

In order to balance these conditions for a good bioink, we prepared a supramolecular hydrogel-based bioink with good rheological and tunable mechanical properties, and exploited this bioink in 3D bioprinting technology. Specifically, chitosan and gelatin are chosen as the main body because of their innate biodegradability and biocompatibility [15,16]. Polyethylene glycol (PEG) was introduced as sidechains of chitosan for two purpose: a) making chitosan water soluble, and b) forming PPR structure with α -cyclodextrin (α -CD). The increased viscosity resulting from gelatin and the aggregation of PPR structure provide good shear-thinning property for the supramolecular hydrogel. This supramolecular hydrogel encapsulated with cells could be processed in 3D bioprinting. Most importantly, tunable strength of the bioink can be obtained by using different concentration of β -Glycerophosphate solution (β -GPS) as the secondary crosslinking agent. The strength tunable bioink was further detected for influencing stem cell differentiation. This work provides a strategy for the construction of supramolecular hydrogel-based bioink.

2. Materials and methods

All reagents and solvents were used as received from commercial sources. Chitosan (molecular weight: 200000 Da, degree of deacetylation: $\geq 90\%$) was purchased from Yunzhou Biochemistry Co., Ltd (Qingdao, China). Polyethylene Glycol Monomethyl Ether 2000 (mPEG-OH 2000, P2186) was obtained from Tokyo Chemical Industry (TCI). N-(3-Dimethylaminopropyl)-N'-ethylcarbodiimide hydrochloride (EDC·HCl, 7084-11-9), N-hydroxysulfosuccinimide (NHS, H109337), 2-(N-morpholino) ethanesulfonic acid (MES, M163014), Succinic anhydride (S104823) and α -cyclodextrin (α -CD, C106777) were purchased from Aladdin Biochemical Technology Co., Ltd (Shanghai, China). Gelatin from porcine skin (Type A, G1890) was obtained from Sigma-Aldrich. N, N-Dimethylformamide (DMF, A39494) was purchased from Inno-chem. β -Glycerophosphate (G9140) was obtained from Solarbio (Beijing, China).

2.1. Preparation of mPEG-COOH

mPEG-OH 2000 (10 g, 5 mmol) was dissolved in 40 ml DMF. Succinic anhydride (1 g, 10 mmol) was added after being dissolved completely. The reaction was allowed to proceed at 60 °C for 15 h under the protection of nitrogen. After cooling to room temperature, the excess solvent was removed using rotary evaporator and the obtained product was dissolved with dichloromethane. The solution was precipitated in excess anhydrous diethyl ether and the product was collected by suction filtration. Ultimately, the obtained product was washed three times by excess anhydrous diethyl ether and dried in the vacuum drying chamber to obtain mPEG-COOH.

2.2. Preparation of CS-mPEG

Firstly, chitosan (0.1 g, 0.62 mmol glucose units) was dissolved in 20 ml MES solution (25 mM, pH = 5.46) by adding HCl solution (0.1 M). Next, EDC·HCl (0.476 g, 2.48 mmol), NHS (0.286 g, 2.48 mmol) and mPEG-COOH (1.303 g, 0.62 mmol) were added in 10 ml MES solution. The solution was allowed to proceed for 30 min in order to activate carboxyl group. Then, the two solutions were mixed and stirred at room temperature for 24 h in the dark. Finally, the solution after the reaction was dialyzed ($M_w^{\text{cut off}} = 3500$ Da) against with deionized water for 3 d. CS-mPEG was obtained as a white porous sponge by lyophilization.

2.3. Preparation of hydrogel and bioink

According to the solubility of modified chitosan and previous study [17] in our group, 0.3 g CS-mPEG and 0.3 g gelatin were dissolved in 10 ml double distilled H₂O with each concentration of 30 mg/ml α -CD was dissolved in double distilled H₂O with concentration of 200 mg/ml for further usage. For the preparation of bioink, 500 μ l cell suspension (cell density 1×10^7 /ml) was added into the hydrogel at this stage. Mix the two solutions at a volume ratio of 3:2 and rest at room temperature for 30 min.

2.4. Structural characterization

NMR spectra was performed on a 400 MHz Bruker NMR spectrometer (Avance-400, Varian) at 25 °C with D₂O as the solvent. FTIR was obtained on a Varian Excalibur 3100 spectrophotometer. XRD pattern was collected on a Bruker X-ray diffractometer (D8 focus, Cu K α , $\lambda = 0.15178$ nm) with the step of 0.1° s^{-1} . After freeze-dried by vacuum freeze-drying at -80°C , the morphology of hydrogel was seen by scanning electron microscopy (SEM) (Hitachi-S4800, Japan) at the voltage of 10 kV.

2.5. Rheological test

The rheology of bioink was tested by rheometer (TA-ARES G2, America) with a coaxial two parallel plates model in which the clamp diameter was 40 mm. Viscosity was measured at shear rate from 0.1 to 100 s^{-1} . The angular frequency sweep was conducted from 0.1 to 100 rad/s at a 5% strain. All measurements were conducted at ambient temperature (25 °C).

2.6. Mechanical test

The mechanical property of bioink was tested on desktop electronic universal material testing machine (Instron 3365, England) with a 100 N load. The cylindrical sample (diameter: 10 mm; height: 1 mm) was used for compression test with a crosshead velocity of 2 mm/s until the sample was broken. Then, we took the first 10% of curve to calculate the slope as the Young's modulus. Each group has five parallel samples. All tests were performed at room temperature (25 °C).

2.7. Porosity measurement

The porosity was measured according to as followed equation in a specific gravity bottle through the ethanol immersion method. Where V_1 is the initial volume of dehydrated alcohol used to submerge the dried hydrogel, V_2 is defined as the total volume of the system when the dried hydrogel is immersed in the dehydrated alcohol, and V_3 is the volume of the residual liquid after the liquid-impregnated hydrogel is removed. Each group has five parallel samples ($n = 5$).

$$\text{Porosity} = (V_1 - V_3) / (V_2 - V_3) \times 100\%$$

2.8. The process of 3D printing

Based on our pervious 3D bioprinting processes [18], the printing was conducted on the bioprinting platform (Regenovo 3D bioprinter, China) with liquid temperature controller (Thermo). 10 ml hydrogel inks were transferred into sterilized a printing syringe. After a cooling process of 30 min in 15 °C, the printing syringe was equipped on the print arm (15 °C) of printing platform, and a 35 mm culture dish was put on the precooled print platform (4 °C). The printing process constructed a 3D columnar with 10 mm diameter and 3 mm thickness, 2 mm interval pores were formed by layer-by-layer pattern of printing nozzle. The bioprinted construct was crosslinked by immersing in β -GPS solution for 10 min at room temperature. The β -GPS solution was replaced by culture medium after crosslinking, the constructs were washed twice with complete culture medium to eliminate any residue crosslinking agent. Finally, the bioprinted constructs were cultured in DMEM with 10% fetal bovine serum (FBS) in an incubator at 37 °C and a humidified atmosphere of 5% CO₂.

2.9. Cell culture and CCK8 assay

2.9.1. Fibroblasts isolation and culture

All animal procedures were approved by the Institutional Animal Care and Use Committee of Chinese PLA General Hospital (Beijing, China), and all the authors who conducted animal experiment were in compliance with all relevant ethical regulations. C57BL/6 mice were used for isolation of dermal fibroblasts. C57 mice were purchased from SPF Biotechnology (Beijing, China). The procedure followed a published protocol [19]. Briefly, newborn mice were killed by immersion in betadine for 2 min then rinsed with deionized water. The skin was pulled from the newborn mice then placed and floated on trypsin (T1300, Solarbio) overnight at 4 °C. The epidermis and dermis were separated with tweezers and the epidermis was discarded. Then the dermis was rinsed with complete Dulbecco's modified Eagle medium (DMEM; SH30243.01, Hyclone) containing 10% fetal bovine serum (FBS; 10437028, Gibco). Rinsed dermises were transferred in sterile centrifuge tubes and 2 ml of 0.35% collagenase (C8140, Solarbio) was added per dermis. The dermises were incubated and agitated in a shaking incubator at 37 °C with low speed for 40 min. The suspension was neutralized with complete DMEM with 10% FBS, and passed through a cell strainer (431752, Corning) to centrifuge at 1500 rpm for 5 min. The pellet contained dermal fibroblasts which were resuspended with DMEM medium and used to seed culture dishes. All operations took place under sterile conditions.

2.9.2. Mesenchymal stem cells isolation, culture, and differentiation

C57 mice were purchased from SPF Biotechnology (Beijing, China). Based on previous studies from other labs and our group [20–22], second passage cells from postnatal mice (male, 7 day old) were used for this study. 7-days-old mice were culled and immersed in 75% ethanol for 10 min. Bilateral femurs and tibias were removed from the mice aseptically. Bones were placed in a sterile 100 mm dish containing complete MesenCult™ Expansion Medium (Mouse) (#05513,

STEMCELL™). Bones were crushed with haemostatic forceps by enough force to crack them. Then bone cracks were gently agitated to free the bone marrow. Finally the medium containing bone marrow was filtered through a 70 μ m cell strainer (BD Falcon). Freshly isolated cells were plated in 100 mm dishes and cultured at 37 °C, 5% CO₂. Media were replaced after 72 h, and cells were passaged when confluent about 80%. MSCs were collected and mixed with bioink as the methods mentioned in the 3D bioprinting process, the bioprinted constructs were cultured in MesenCult™ Adipogenic Differentiation Kit (#05507, STEMCELL™) medium and NeuroCult™ Differentiation Kit (#05704, STEMCELL™) medium for adipogenic and neural differentiation. Differentiation medium was replaced every three days until the endpoint time for collection.

2.9.3. CCK-8 assay

A Cell Counting Kit 8 (CA1210, Solarbio, Beijing, China) was used in all CCK-8 experiments. Cells were incubated in 25 cm² cell-culture flasks. When cell confluent reaches 80%, cells (1×10^4 cells/well) were seeded into a 96-well plate with volume of 100 μ l of medium for each well. Cells were exposed to various component of bioinks for 24 h (for CS-mPEG, and α -CD), or certain time points for β -GPS. 10 μ l CCK-8 solution was added into each well. Standard curve was established for each experiment. The cell viability was calculated as the ratio of the absorbance at 450 nm of the wells compared with standard curve. The absorbance at 450 nm was measured using a Thermo Multiskan FC multplate photometer.

2.10. Immunofluorescent staining and specific staining

Bioprinted constructs were embedded in Optimal Cutting Temperature (O.C.T.) Compound (Sakura) and frozen at -30 °C. 7 μ m sections were obtained by freezing microtome (Leica) and fixed by 10% formalin for 30 min. Specific markers were used to stain sections according to standard immunofluorescence protocols. Briefly, sections were incubated overnight at 4 °C with primary antibodies [rabbit monoclonal anti-beta actin (1:300, ab8227, Abcam), anti-paxillin (1:250, ab32084, Abcam), Ki67 (1:250, ab16667, Abcam), N-cadherin (1:300, ab18203, Abcam)] after antigen retrieval, and blocking. Sections were immersed with the goat anti-rabbit secondary antibody Alexa Fluor® 488 (1:300, ab150077, Abcam) and CoraLite594 goat anti-mouse IgG (1:300, SA00013-3, proteintech) for 2 h in the dark at room temperature. Finally, incubated sections were mounted in DAPI Fluoromount-G (0100-20, Southern Biotech) and pictures were taken with a fluorescence microscope (Olympus, BX51) within 24 h. Mean fluorescence intensity was measured from three random figures in one group by mean grey value from ImageJ.

2.10.1. Oil Red staining

Oil Red staining were conducted by the instruction of Oil Red O (ORO) staining kit (G1262, Solarbio, Beijing, China). Briefly, 15 μ m sections of bioprinted constructs were freshly cut by freezing microtome. Slices were fixed by ORO Fixative for 10–15 min, and put in ventilated space for another 10 min. Immersed the slices into freshly prepared ORO Stain for 15 min, then washed by isopropanol for 20–30 s, and finally washed by distilled water thoroughly. Nuclear was counterstained with Mayer hematoxylin for 2 min. Slices were processed with ORO Buffer for 1 min and mounted by glycerine/gelatin mounting medium.

2.10.2. Nissl Body Staining

Methylene blue staining was used to identify Nissl body by Nissl Body Staining kit (G1434, Solarbio, Beijing, China). The staining was conducted with the instruction of the kit. Briefly, bioprinted constructs were embedded in O.C.T. and cut into 5 μ m sections, followed by fixation with 10% formalin for 15 min. Drop the Methylene Blue Stains on the slices and stained for 10 min. Immersed the slices into Nissl

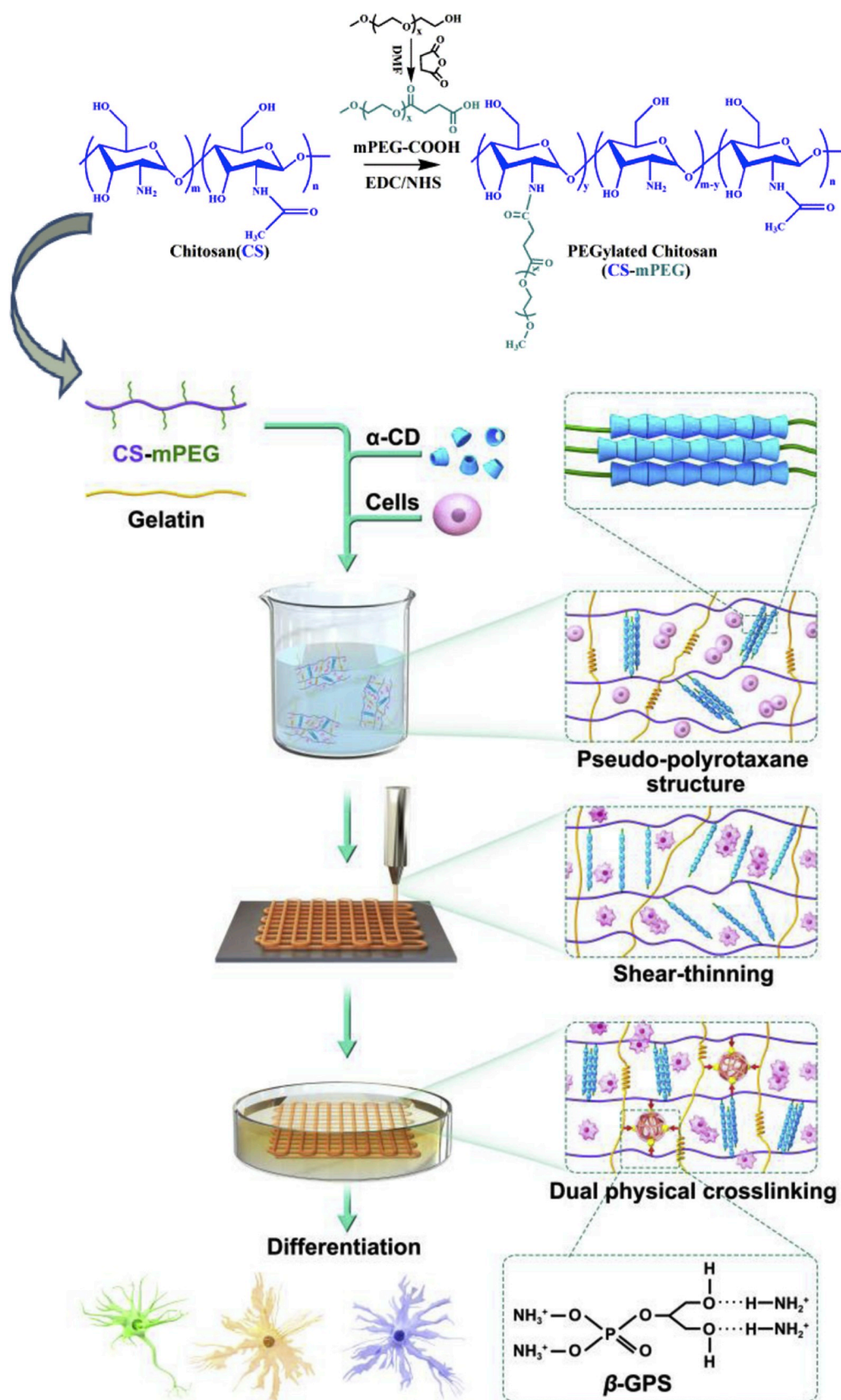


Fig. 1. Schematic illustration and flow chart of CS-mPEG formulation, bioink preparation, dual physical crosslinking, and 3D bioprinting process.

Differentiation solution, and observed the Nissl body under microscopy. Immersed the slices with Ammonium Molybdate solution for 3 min, and washed them with distilled water. Processed with routine dehydration and transparency, and mounted with neutral resins.

2.11. Statistic analysis

All numeric data in the study are demonstrated as mean \pm standard deviation, and analysed with Student's t-test and one-way ANOVA in GraphPad Prism version 8 and SPSS version 26. $P < 0.05$ is regarded as statistical significance.

3. Results and discussion

3.1. Formation of PPR structure and the rheological behavior of bioink

PEGylated chitosan (CS-mPEG) was prepared as Fig. 1 shows. The methoxy polyethylene glycol (mPEG) was firstly carboxylated, and then the obtained carboxymethoxypolyethylene glycol (mPEG-COOH) was conjugated to the amino groups of chitosan through an EDC/NHS-mediated coupling reaction. The chemical structures were assessed by ^1H -Nuclear Magnetic Resonance (^1H NMR), Fourier Transform Infrared Spectroscopy (FTIR) and X-Ray Diffraction (XRD). From ^1H NMR spectra (Fig. S1), the appearance of peak 1 in Fig. S1d is the characteristic peak of $-\text{OCH}_3$, which proves the successful synthesis of CS-mPEG. The degree of substitution (DS) was calculated by counting the peak value of $-\text{OCH}_3$ which was located in the side chain of CS-mPEG. The DS of the obtained CS-mPEG was determined to be 0.82. It also showed that there were residual amino groups in chitosan. As indicated in FTIR spectrum (Fig. 2a), the absorbance at 1736 cm^{-1} , which is the characteristic peak of $\text{C}=\text{O}$, confirmed the formation of the mPEG-COOH. The absorbance at 1736 cm^{-1} was weakened in the CS-mPEG. It indicated that amino groups of chitosan reacted with the carboxyl groups of mPEG-COOH. From XRD spectra (Fig. 2b), unmodified chitosan showed a strong reflection at $2\theta = 20^\circ$. This indicated that there

were some regular crystal regions in chitosan, which are mainly related to the large number of intramolecular and intermolecular hydrogen bonds. The characteristic peak disappeared with the incorporation of PEG, while two strong reflections appeared around $2\theta = 19^\circ$ and 23° , which come from the ordered arrangement of ethylene oxide units of PEG. These results confirmed the synthesis of CS-mPEG.

The PPR structure was formed by mixing CS-mPEG solution with α -CD solution. After freeze-drying, the structure was determined by FTIR (Fig. 2a). The absorbance at 3395 cm^{-1} became wide because of a large number of hydroxyl group of α -CD. Moreover, the absorbance at 1153 cm^{-1} , 1030 cm^{-1} was also characteristic peak of α -CD. The XRD pattern (Fig. 2b) of the supramolecular hydrogel revealed two characteristic diffractions at $2\theta = 19.96^\circ$ and 22.56° consistent with other studies on the inclusion complex of α -CD, indicating the supramolecular hydrogel with a channel-type crystalline structure [12,23].

By stirring the CS-mPEG/ α -CD complex vigorously and waiting for several minutes, the aggregation of the PPR-like side chains induced the formation of supramolecular hydrogel (Fig. S2). Storage modulus (G') and loss modulus (G'') of supramolecular hydrogel was tested by time scanning. G' and G'' reach the intersection point within 80 s (Fig. 2c). After this point, G' value is always higher than G'' value, indicating that the supramolecular hydrogel has been formed. The result demonstrated that the supramolecular hydrogel has a fast gelation time, which is beneficial for the preparation of bioink and mixture with cells.

Rheological property plays key roles for the bioink. To achieve improved viscosity and gelling property, the prepared CS-mPEG/ α -CD supramolecular hydrogel was blended with gelatin. The viscosity of the obtained CS-mPEG/ α -CD/gelatin bioink was tested. Due to the reversibility of the PPR-based physical crosslinking and the hydrogen bond-based physical crosslinking of gelatin, the viscosity of the bioink decreased with increasing shear rate (Fig. 2d). This shear-thinning property implied that this bioink is suitable for extrusive printing through nozzle. Frequency scanning (Fig. 2e) revealed that the value of G' is higher than that of G'' within an angular frequency range of 0.1–100 rad/s. The large difference between G' and G'' enables the

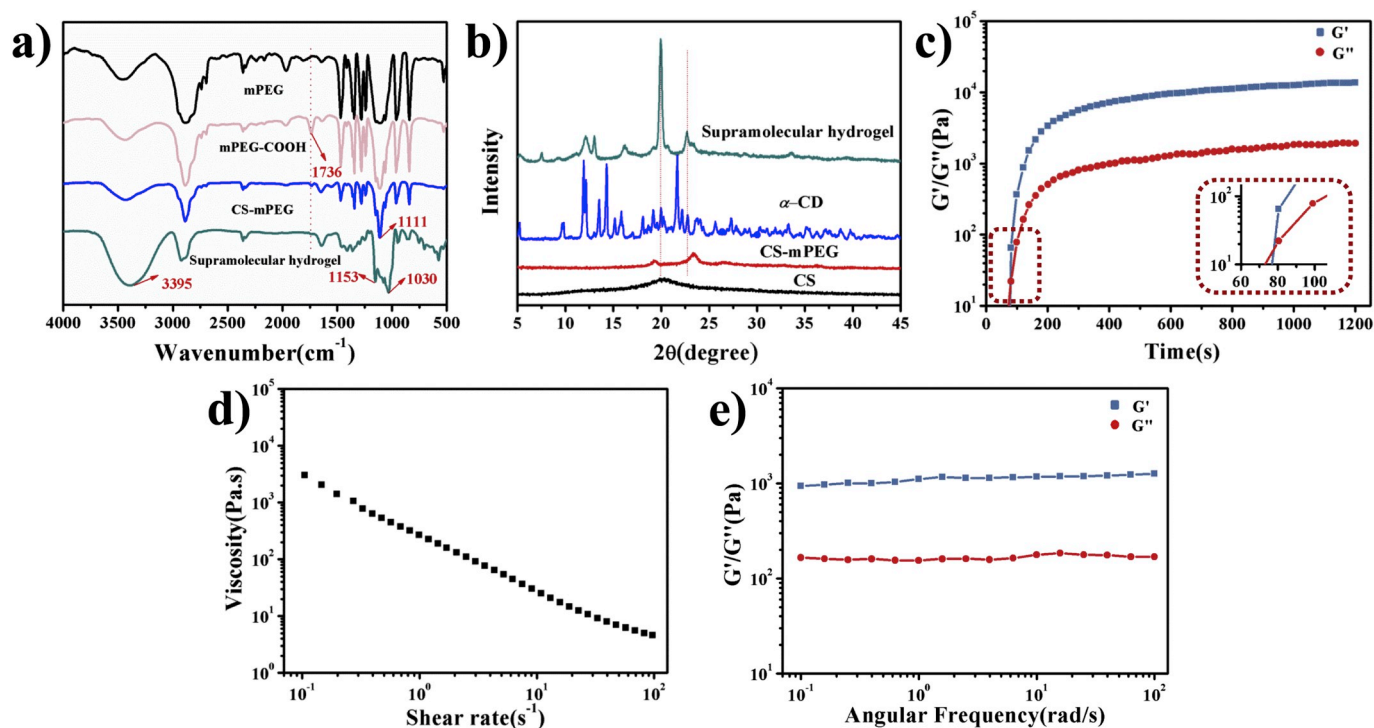


Fig. 2. Structural characterization and rheological properties of supramolecular hydrogel-based bioink. a) FTIR spectra of bioink main components. b) XRD patterns. c) G' and G'' at an angular frequency of 1 Hz at 25°C . d) Apparent viscosity of bioink under steady shear from 0.1 s^{-1} to 100 s^{-1} at 25°C . e) G' and G'' under steady angular frequency from 0.1 rad/s to 100 rad/s and an oscillatory strain of 5% at 25°C .

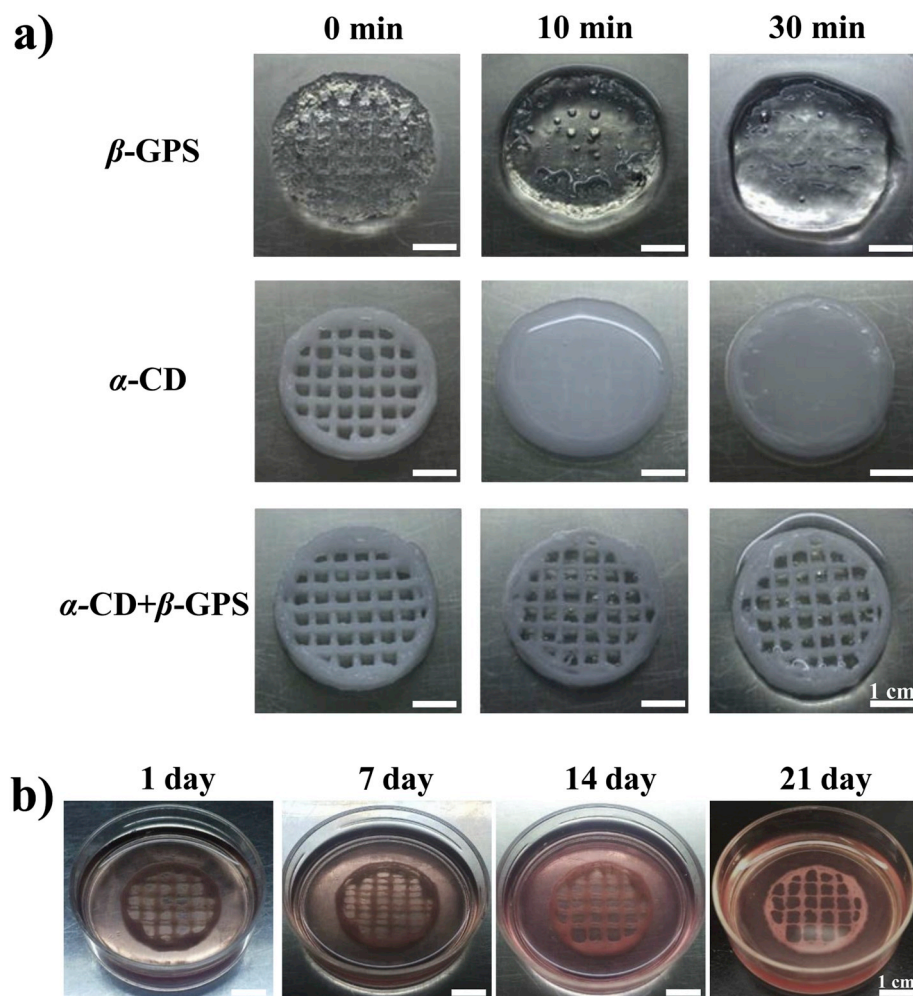


Fig. 3. Printability and stability of bioprinted constructs. a) Macroscopy image of bioprinted constructs crosslinked by dual physical crosslinking (β -GPS and α -CD) or single crosslinking (only β -GPS or α -CD). α -CD was added in the bioinks during preparation as described in the Methods section. b) Macroscopy image of dual-crosslinked and cell-laded bioprinted constructs cultured in medium under the condition of normal cell culture.

stable flow of the bioink in the extrusion process.

The aggregation of PPR-like side chains in supramolecular hydrogel and helical structure in gelatin temporarily disintegrated when the bioink is under shear force, which allows it to be extruded. The broken structure could automatically form again leading to recovering original stable condition after the removal of shear force. As a result, the bioink exhibits good printability and self-recovery property. This property highlights its advantages in application of 3D bioprinting, especially compared with traditional hydrogel which are crosslinked by immutable covalent-bonds [17–20].

3.2. Bioprinting process and tunable mechanical properties

The prepared CS-mPEG/ α -CD/gelatin bioink was bioprinted through an extrusive 3D bioprinter. Then, the obtained constructs were subsequently immersed into β -GPS solution for the secondary crosslinking. To observe the stability of the bioprinted constructs by dual physical crosslinking, post-printed constructs with only α -CD or with only β -GPS were prepared for comparison. The structure of bioprinted constructs with only one crosslinking agent deformed after a short time (Fig. 3a). It clearly showed that the constructs with dual physical crosslinking could maintain the shape after printing and remain the structure under cell culture condition for at least 21 days (Fig. 3b). This indicated that the bioprinted construct could form a stable structure due to dual physical crosslinking, and is also eligible for cell culture.

Strength and porosity of bioink will exert power effects on cellular behaviours and biological results, ranging from mechanical signalling, cellular skeleton and geometry, transcriptional expression, to cell viability, proliferative activity, and differentional trajectory. In this study, the strength and porosity of the bioink can be regulated by different concentration of β -GPS. The strength of 3D scaffolds increased with the concentration of β -GPS (Fig. 4a). Yong's modulus was also tested for long time cell culture, Fig. 4b showed fully crosslinked bioprinted constructs could maintain their strength for at least 21 days. Under different concentration of β -GPS, the Young's modulus ranged from 4 kPa to 130 kPa. The porosity (Fig. 4c) shows the opposite trend, which demonstrated it decreased along with the increase of β -GPS concentration. The results of SEM analysis showed that the size of pore decreases gradually with the increase of crosslinking agent concentration (Fig. 4d).

Shear-thinning and self-recovery hydrogels have been designed and investigated in many recent publications. Claudia Loebel et al. [24] developed a group of hyaluronic acid-based hydrogels through guest–host interactions. The interaction between guest moieties of adamantanes and host moieties of β -cyclodextrins underlies the capability of shear-thinning and self-recovery. In keeping with Claudia Loebel's work, the properties of disassembling and re-forming in our supramolecular hydrogel have been tested in this study. In addition to guest–host interaction, the secondary crosslinking by β -GPS reinforce the weak mechanical strength of this supramolecular hydrogel, which

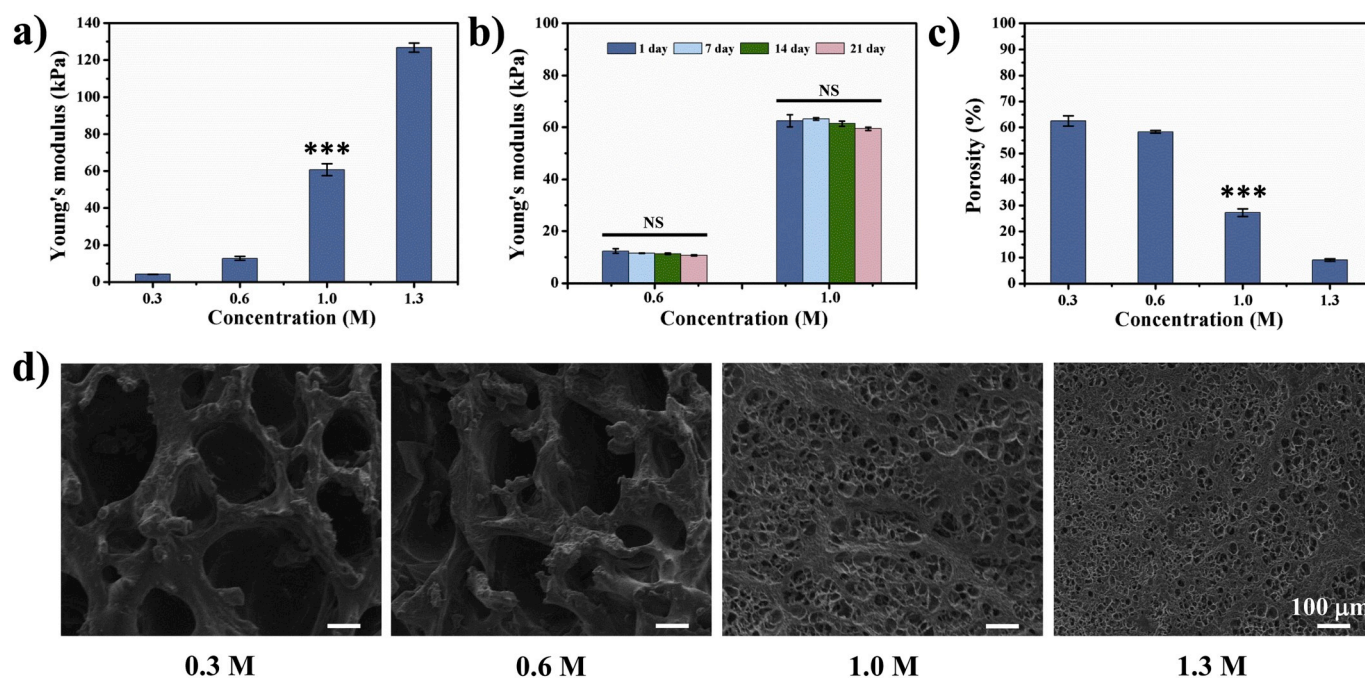


Fig. 4. The mechanical properties of bioprinted constructs crosslinked in different concentration of β -GPS. a) Young's modulus of bioprinted constructs with β -GPS in 0.3 M, 0.6 M, 1.0 M, and 1.3 M. b) Young's modulus for the bioprinted constructs with β -GPS in 0.6 M and 1.0 M in cell culture condition on 1 day, 7 days, 14 days, 21 days. c) Porosity of bioprinted constructs crosslinked with β -GPS in 0.3 M, 0.6 M, 1.0 M, and 1.3 M. d) The images of SEM for bioprinted constructs crosslinked with β -GPS 0.3 M, 0.6 M, 1.0 M, and 1.3 M after freeze-drying. *** indicates significant statistical difference ($p < 0.001$) with those of group of 0.6 M; NS indicates no statistical significance.

has been a long time limitation of guest-host based hydrogels [13,25,26]. In this study, the secondary crosslinking agent are rationally designed to solve the problem of weak mechanical strength. Phosphate groups of β -GPS could form ionic bonds and hydrogen bonds with amidogen in chitosan and gelatin. In addition, the compression Young's modulus of dual crosslinked bioink increases with the rising concentration of β -GPS, along with the declining of porosity.

3.3. Cellular proliferation and adhesion in bioprinted constructs

Before the bioprinting process, cellular toxicity was tested by co-culturing fibroblasts with each component of bioink. CCK-8 assay demonstrated cell viability of cells with each component is higher than 80%, which is regarded as biocompatible (Fig. 5). Fibroblast-laden bioink underwent bioprinting with 1.0 M β -GPS as the crosslinking agent, and bioprinted constructs were cultured for 14 days. Quantification of immunofluorescence results demonstrated that the expression of Ki67 was higher in 14 days than those of 7 days when bioprinted and cultured with bioink (Fig. 6). As a cellular protein expressed during mitosis, Ki67 is used as a specific marker for cellular proliferation.

As a member of the cellular skeleton system, actin was used in the immunofluorescence to identify cell spreading and outline. Fig. 6a indicates that fibroblasts can express actin normally and maintain physiological cellular shape. Paxillin and N-cadherin are involved into the formation of complex protein structures of cell-matrix adhesion and cell-cell adhesion. Fig. 6a and b showed that cells in bioprinted constructs could not only express these adhesion markers, but also increase the expression levels of these markers along with the culture time.

Bioprinted constructed could not only provide a more biomimetic extracellular matrix for the residing cells, but also the biophysical and surface topographical properties would boost cellular behaviours, such as cell proliferation, adhesion, spreading, and assembly. The possible reason for the increased expression of Ki67 might be the mechanical properties and roughness of the surface topography, which are reported to stimulate mitogenic signalling pathway or activate Rac/FAK

[27–31]. Through activating mechanotransduction receptors and cellular skeleton remodelling, cell proliferation are found to relate with these properties of extracellular matrix [32,33].

Cellular survival rate, adhesion, and proliferation are three cardinal indexes among all the cellular behaviours to represent overall cell condition in the detection of biocompatibility. Our results demonstrated good biocompatibility of fibroblasts in this bioink both in co-culture and bioprinted condition. Promoting cellular biocompatibility has been researched for a long time in the application of various sorts of biomaterials. Some ideal materials, mechanically or economically, suffer from poor biocompatibility that hinder their ability in biomedical application. Good performance of cellular behaviours in this supra-molecular hydrogel-based bioink provide empirical and theoretical evidence for further application. One major theoretical issue that has dominated the field of many years concerns maintaining mechanical properties of biomaterials without loss of biocompatibility, which has been investigated by many studies [34–36]. With well-known good biocompatibility, PEG and α -CD are incorporated into the bioink not only for the host-guest interaction but also for the concerns of future application. As a novel bioink, its further application is conditioned by this theoretical issue.

3.4. Mesenchymal stem cells differentiation in strength tunable 3D constructs

Bone marrow-derived mesenchymal stem cells (MSCs) were isolated to test the effect of strength tunable 3D bioprinted structure on stem cell differentiation. Mixed with supramolecular hydrogel-based bioink, MSCs were bioprinted with different level of crosslinking agent. Given the strength range of this bioink that mentioned above and related studies, 0.6 M and 1.0 M of β -GPS were chosen to produce bioprinted extracellular matrix with two different strength. It is reported that the Young's modulus of 10–20 kPa and 60–200 kPa are in favor of neural and adipose lineage differentiation of MSCs, respectively [37–42]. Oil Red O specific staining demonstrated few lipid droplet containing cells

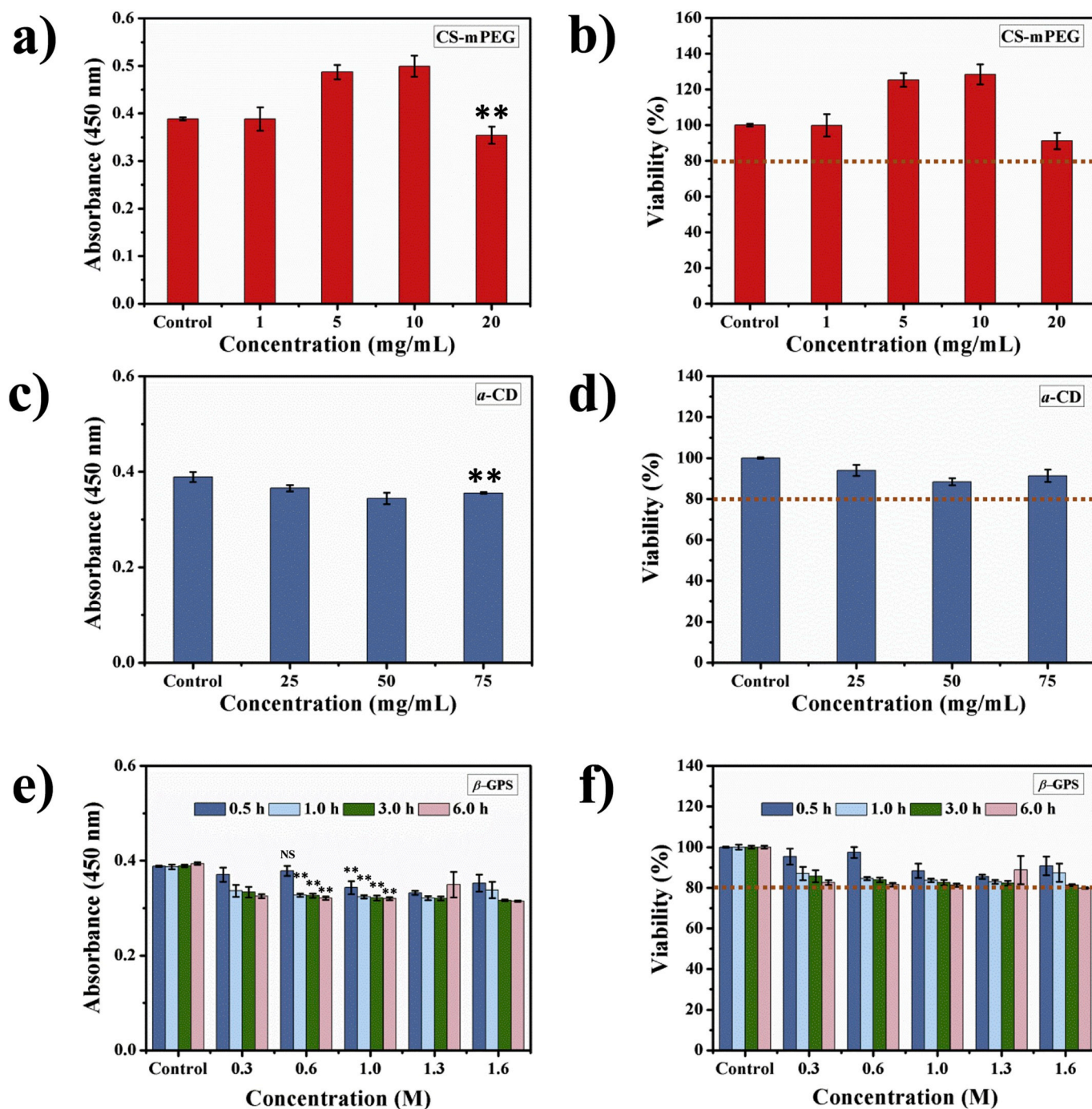


Fig. 5. The *in vitro* cytotoxicity assay of main components and fibroblast by CCK-8. a) Raw absorbance of CCK-8 assay and b) percent of viability of fibroblasts co-cultured with different concentrations of CS-mPEG. c) Raw absorbance of CCK-8 assay and d) percent of viability of fibroblasts co-cultured with different concentrations of α -CD. e) Raw absorbance of CCK-8 assay and f) percent of viability of fibroblasts co-cultured with different concentrations of β -GPS for 0.5 h, 1.0 h, 3.0 h, and 6.0 h. A viability of higher than 80% is normally acceptable for biomaterials with good biocompatibility ** indicates statistical significance ($p < 0.01$) when compared with corresponding control group; NS indicates no statistical significance.

could be observed in bioprinted structure with 0.6 M β -GPS (Fig. 7a). In bioprinted construct with 1.0 M β -GPS, Oil red staining positive cells were significant after 21 days of culture, which implied bioink in 60 kPa may promote MSCs differentiation towards adipose cells, when compared with those of bioink in 10–20 kPa. Quantification of specific staining demonstrated the impact in Fig. 7c.

Nissl body staining was used to specifically identify neuron cells or neuron-like cells. As demonstrated in Fig. 7b, cells in bioink with 0.6 M β -GPS indicated more significant positive staining than those in 1.0 M β -GPS, with quantification data in Fig. 7d. The results manifested bioink

with Young's modulus of 10–20 kPa could facilitate MSCs differentiation towards neural cells when compared with those of bioink in strength of 60 kPa.

Mechanistic cues have been proved to be one of the irreplaceable biophysical stimuli to cells in both physiological and pathological condition [43,44]. In bioengineering area, this property is adopted by researchers to manipulate stem cell differentiation, and targeted stem cell differentiation serves as one approach in therapeutical studies and regenerative medicine [45–48]. Our results showed this bioink could be used to prepare strength tunable 3D constructs without alteration of the

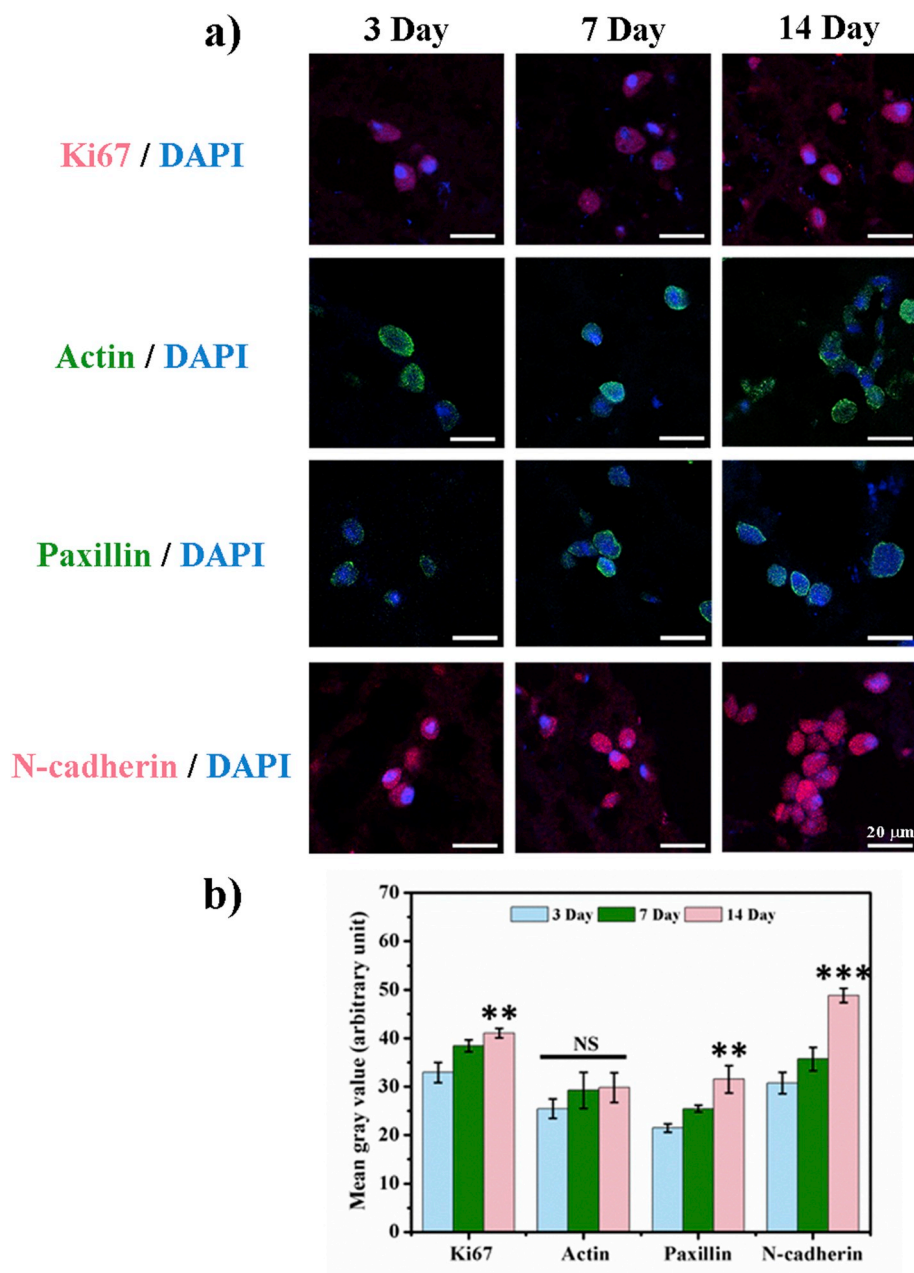


Fig. 6. Immunofluorescence staining of cellular proliferation and adhesion in cells bioprinted with the supramolecular bioink. a) Expression of Ki-67, Actin, Paxillin, and N-cadherin in fibroblasts bioprinted with bioink after 3, 7, and 14 days of culture (scale bar = 20 μm). b) Quantification of the immunofluorescence intensity per area by mean grey value from three random pictures. ** and *** indicate statistical significance ($p < 0.01$, and $p < 0.001$, respectively) when compared with those in day 3. NS indicates no statistical significance.

main components. Many studies published their findings that bioink with different strength can precisely monitor stem cell differentiation, but alternative strength is accomplished by different proportion or concentration of the main components [41,49]. In the current study, tunable strength can be achieved only by adjusting concentration of the secondary crosslinking agent, which implicates the possibility to simultaneously drive stem cell differentiation towards distinctive lineages in a same bioprinted system. And the corresponding results of stem cell differentiation have also proved the feasibility and capability of this strength tunable bioink.

One of the ultimate goals in bioprinting technology is to construct complicated organs which are usually composed of assorted types of tissue and cells. The majority studies of bioink focus on the promoted properties or translational application for some specific tissues or cell

types, as Table S1 have displayed some main categories of extrusive bioink with their formulation, advantages and disadvantages. Besides, it is difficult to bioprint miscellaneous cells without changing the components of bioink. The supramolecular hydrogel based bioink in this study provide a possibility to establish distinctive cells *in vitro*.

4. Conclusion

In summary, we have successfully prepared a novel supramolecular hydrogel-based bioink which composed of PEGylated chitosan, gelatin, α -CD, and β -GPS. A stable bioprinted constructs is obtained via dual physical crosslinking without toxic byproducts or hazardous components during all the above processes. The bioink exhibited not only ideal biocompatibility but also tunable strength. The primed

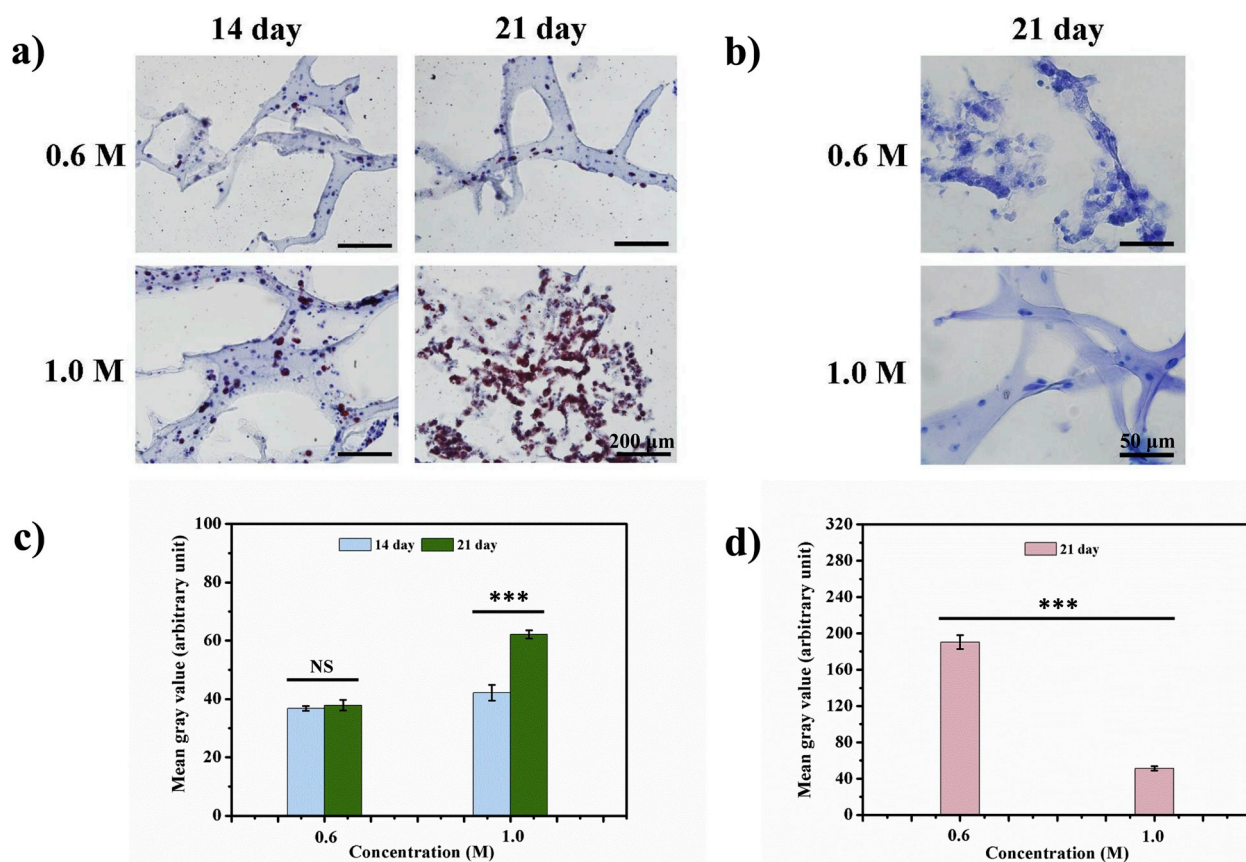


Fig. 7. Adipose and neural cell specific staining for bioprinted MSCs in bioink with different concentration of β -GPS. a) Oil Red O staining for bioprinted MSCs in bioink with 0.6 M and 1.0 M β -GPS after 14 and 21 days of culture. The orange and red color indicates lipid droplets inside cells. (scale bar = 200 μ m); b) Nissl body specific staining for bioprinted MSCs in bioink with 0.6 M and 1.0 M β -GPS after 21 days of culture. The blue color indicates large extranuclear RNA granules in neurons or neuron-like cells (scale bar = 50 μ m). Quantification of c) Oil red and d) Nissl body specific staining was performed by mean gray value from three random pictures. *** indicates statistical significance ($p < 0.001$). NS indicates no statistical significance. (For interpretation of the references to color in this figure legend, the reader is referred to the Web version of this article.)

mechanical properties were further tested for influencing MSCs differentiation towards adipose and neural lineage in strength tunable bioinks. The obtained relationship between the concentration of crosslinking agent and tunable strength might provide new avenue for further development of bioinks.

CRedit authorship contribution statement

Tian Hu: Conceptualization, Methodology, Formal analysis, Investigation, Writing - original draft. **Xiaoliang Cui:** Conceptualization, Methodology, Formal analysis, Investigation, Visualization. **Meng Zhu:** Resources. **Man Wu:** Methodology, Resources. **Ye Tian:** Writing - review & editing. **Bin Yao:** Methodology, Formal analysis. **Wei Song:** Investigation, Resources. **Zhongwei Niu:** Writing - review & editing, Supervision, Project administration. **Sha Huang:** Writing - review & editing, Supervision, Project administration. **Xiaobing Fu:** Supervision, Funding acquisition.

Declaration of competing interest

The authors declare no conflicts of interest.

Acknowledgements

This work was supported by the National Key Research Development Plan of China (2017YFC1103300), the National Nature Science Foundation of China (81571909, 81701906, 81830064,

81721092, 51703230, and 31971303), the CAMS Innovation Fund for Medical Sciences (CIFMS, 2019-I2M-5-059) and the Military Medical Research and Development Projects (AWS17J005), Fostering Funds of Chinese PLA General Hospital for National Distinguished Young Scholar Science Fund (2017-JQPY-002), Chinese PLA General Hospital for Military Medical Innovation Research Project (CX19026), and the Presidential Foundation of Technical Institute of Physics and Chemistry, Chinese Academy of Sciences.

Appendix A. Supplementary data

Supplementary data to this article can be found online at <https://doi.org/10.1016/j.bioactmat.2020.06.001>.

References

- [1] B. Derby, Printing and prototyping of tissues and scaffolds, *Science* 338 (6109) (2012) 921.
- [2] B. Grigoryan, S.J. Paulsen, D.C. Corbett, D.W. Sazer, C.L. Fortin, A.J. Zaita, P.T. Greenfield, N.J. Calafat, J.P. Gounley, A.H. Ta, F. Johansson, A. Randles, J.E. Rosenkrantz, J.D. Louis-Rosenberg, P.A. Galie, K.R. Stevens, J.S. Miller, Multivascular networks and functional intravascular topologies within biocompatible hydrogels, *Science* 364 (6439) (2019) 458.
- [3] Z. Lin, M. Wu, H. He, Q. Liang, C. Hu, Z. Zeng, D. Cheng, G. Wang, D. Chen, H. Pan, C. Ruan, Bioinks: 3D printing of mechanically stable calcium-free alginate-based scaffolds with tunable surface charge to enable cell adhesion and facile bio-functionalization, *Adv. Funct. Mater.* 29 (9) (2019) 1970053.
- [4] S. Ostrovidov, S. Salehi, M. Costantini, K. Suthiwanich, M. Ebrahimi, R.B. Sadeghian, T. Fujie, X. Shi, S. Cannata, C. Gargioli, A. Tamayol, M.R. Dokmeci, G. Orive, W. Swieszkowski, A. Khademhosseini, 3D bioprinting in skeletal muscle tissue engineering, *Small* 15 (24) (2019) 1805530.

- [5] G.-L. Ying, N. Jiang, S. Maharjan, Y.-X. Yin, R.-R. Chai, X. Cao, J.-Z. Yang, A.K. Miri, S. Hassan, Y.S. Zhang, Aqueous two-phase emulsion bioink-enabled 3D bioprinting of porous hydrogels, *Adv. Mater.* 30 (50) (2018) 1805460.
- [6] C. Li, A. Faulkner-Jones, A.R. Dun, J. Jin, P. Chen, Y. Xing, Z. Yang, Z. Li, W. Shu, D. Liu, R.R. Duncan, Rapid formation of a supramolecular polypeptide–DNA hydrogel for In Situ three-dimensional multilayer bioprinting, *Angew. Chem. Int. Ed.* 54 (13) (2015) 3957–3961.
- [7] M. Guvendiren, J. Molde, R.M.D. Soares, J. Kohn, Designing biomaterials for 3D printing, *ACS Biomater. Sci. Eng.* 2 (10) (2016) 1679–1693.
- [8] S.H. Kim, Y.K. Yeon, J.M. Lee, J.R. Chao, Y.J. Lee, Y.B. Seo, M.T. Sultan, O.J. Lee, J.S. Lee, S-i Yoon, I.-S. Hong, G. Khang, S.J. Lee, J.J. Yoo, C.H. Park, Precisely printable and biocompatible silk fibroin bioink for digital light processing 3D printing, *Nat. Commun.* 9 (1) (2018) 1620.
- [9] T. Jungst, W. Smolan, K. Schacht, T. Scheibel, J. Groll, Strategies and molecular design criteria for 3D printable hydrogels, *Chem. Rev.* 116 (3) (2016) 1496–1539.
- [10] G. Wenz, B.-H. Han, A. Mueller, Cyclodextrin rotaxanes and polyrotaxanes, *ChemInform* 37 (24) (2006).
- [11] T. Ooya, H.S. Choi, A. Yamashita, N. Yui, Y. Sugaya, A. Kano, A. Maruyama, H. Akita, R. Ito, K. Kogure, H. Harashima, Biocleavable Polyrotaxane–Plasmid DNA polyplex for enhanced gene delivery, *J. Am. Chem. Soc.* 128 (12) (2006) 3852–3853.
- [12] Z. Tian, C. Chen, H.R. Allcock, Injectable and biodegradable supramolecular hydrogels by inclusion complexation between poly(organophosphazenes) and α -cyclodextrin, *Macromolecules* 46 (7) (2013) 2715–2724.
- [13] D. Chimene, R. Kaunas, A.K. Gaharwar, Hydrogel bioink reinforcement for additive manufacturing: a focused review of emerging strategies, *Adv. Mater.* 32 (1) (2020) e1902026.
- [14] X. Wang, C. Wei, B. Cao, L. Jiang, Y. Hou, J. Chang, Fabrication of multiple-layered hydrogel scaffolds with elaborate structure and good mechanical properties via 3D printing and ionic reinforcement, *ACS Appl. Mater. Interfaces* 10 (21) (2018) 18338–18350.
- [15] L. Elviri, R. Foresti, C. Bergonzi, F. Zimetti, C. Marchi, A. Bianchera, F. Bernini, M. Silvestri, R. Bettini, Highly defined 3D printed chitosan scaffolds featuring improved cell growth, *Biomed. Mater.* 12 (4) (2017) 045009.
- [16] H. Li, Y.J. Tan, L. Li, A strategy for strong interface bonding by 3D bioprinting of oppositely charged κ -carrageenan and gelatin hydrogels, *Carbohydr. Polym.* 198 (2018) 261–269.
- [17] M. Zhu, P. Liu, H. Shi, Y. Tian, X. Ju, S. Jiang, Z. Li, M. Wu, Z. Niu, Balancing antimicrobial activity with biological safety: bifunctional chitosan derivative for the repair of wounds with Gram-positive bacterial infections, *J. Mater. Chem. B* 6 (23) (2018) 3884–3893.
- [18] B. Yao, T. Hu, X. Cui, W. Song, X. Fu, S. Huang, Enzymatically degradable alginate/gelatin bioink promotes cellular behavior and degradation in vitro and in vivo, *Biofabrication* 11 (4) (2019) 045020.
- [19] U. Lichti, J. Anders, S.H. Yuspa, Isolation and short-term culture of primary keratinocytes, hair follicle populations and dermal cells from newborn mice and keratinocytes from adult mice for in vitro analysis and for grafting to immunodeficient mice, *Nat. Protoc.* 3 (5) (2008) 799–810.
- [20] Y. Wang, R. Wang, B. Yao, T. Hu, Z. Li, Y. Liu, X. Cui, L. Cheng, W. Song, S. Huang, X. Fu, TNF- α suppresses sweat gland differentiation of MSCs by reducing FTO-mediated m(6)A-demethylation of Nanog mRNA, *Sci. China Life Sci.* 63 (1) (2020) 80–91.
- [21] J.D. Kretlow, Y.Q. Jin, W. Liu, W.J. Zhang, T.H. Hong, G. Zhou, L.S. Baggett, A.G. Mikos, Y. Cao, Donor age and cell passage affects differentiation potential of murine bone marrow-derived stem cells, *BMC Cell Biol.* 9 (2008) 60.
- [22] C.C. Tsai, P.F. Su, Y.F. Huang, T.L. Yew, S.C. Hung, Oct4 and Nanog directly regulate Dnmt1 to maintain self-renewal and undifferentiated state in mesenchymal stem cells, *Mol. Cell.* 47 (2) (2012) 169–182.
- [23] W. Ha, J. Yu, X-y Song, J. Chen, Y-p Shi, Tunable temperature-responsive supramolecular hydrogels formed by prodrugs as a codelivery system, *ACS Appl. Mater. Interfaces* 6 (13) (2014) 10623–10630.
- [24] C. Loebel, C.B. Rodell, M.H. Chen, J.A. Burdick, Shear-thinning and self-healing hydrogels as injectable therapeutics and for 3D-printing, *Nat. Protoc.* 12 (8) (2017) 1521–1541.
- [25] Z. Wei, J.H. Yang, Z.Q. Liu, F. Xu, J.X. Zhou, M. Zrinyi, Y. Osada, Y.M. Chen, Novel biocompatible polysaccharide-based self-healing hydrogel, *Adv. Funct. Mater.* 25 (9) (2015) 1352–1359.
- [26] V. Yesilyurt, M.J. Webber, E.A. Appel, C. Godwin, R. Langer, D.G. Anderson, Injectable self-healing glucose-responsive hydrogels with pH-regulated mechanical properties, *Adv. Mater.* 28 (1) (2016) 86–91.
- [27] Y. Li, Y. Xiao, C. Liu, The horizon of materiobiology: a perspective on material-guided cell behaviors and tissue engineering, *Chem. Rev.* 117 (5) (2017) 4376–4421.
- [28] C.S. Chen, M. Mrksich, S. Huang, G.M. Whitesides, D.E. Ingber, Geometric control of cell life and death, *Science (New York, NY)* 276 (5317) (1997) 1425–1428.
- [29] A.M. Smith, J.Z. Paxton, Y.P. Hung, M.J. Hadley, J. Bowen, R.L. Williams, L.M. Grover, Nanoscale crystallinity modulates cell proliferation on plasma sprayed surfaces, *Mater. Sci. Eng. C Mater. Biol. Appl.* 48 (2015) 5–10.
- [30] R.K. Assoian, E.A. Klein, Growth control by intracellular tension and extracellular stiffness, *Trends Cell Biol.* 18 (7) (2008) 347–352.
- [31] F. Gentile, L. Tirinato, E. Battista, F. Causa, C. Liberale, E.M. di Fabrizio, P. Decuzzi, Cells preferentially grow on rough substrates, *Biomaterials* 31 (28) (2010) 7205–7212.
- [32] F. Guilak, D.M. Cohen, B.T. Estes, J.M. Gimble, W. Liedtke, C.S. Chen, Control of stem cell fate by physical interactions with the extracellular matrix, *Cell Stem Cell* 5 (1) (2009) 17–26.
- [33] Y. Cui, F.M. Hameed, B. Yang, K. Lee, C.Q. Pan, S. Park, M. Sheetz, Cyclic stretching of soft substrates induces spreading and growth, *Nat. Commun.* 6 (2015) 6333.
- [34] C. Lee, J. Shin, J.S. Lee, E. Byun, J.H. Ryu, S.H. Um, D.I. Kim, H. Lee, S.W. Cho, Bioinspired, calcium-free alginate hydrogels with tunable physical and mechanical properties and improved biocompatibility, *Biomacromolecules* 14 (6) (2013) 2004–2013.
- [35] M.C. Darnell, J.Y. Sun, M. Mehta, C. Johnson, P.R. Arany, Z. Suo, D.J. Mooney, Performance and biocompatibility of extremely tough alginate/polyacrylamide hydrogels, *Biomaterials* 34 (33) (2013) 8042–8048.
- [36] K. Luo, Y. Yang, Z. Shao, Physically crosslinked biocompatible silk-fibroin-based hydrogels with high mechanical performance, *Adv. Funct. Mater.* 26 (6) (2016) 872–880.
- [37] Kirsch M, Birnstein I, Pepelanova I, Handke W, Rach J, Seltsam A, Scheper T, Lavrentieva A. Gelatin-methacryloyl (GelMA) formulated with human platelet lysate supports mesenchymal stem cell proliferation and differentiation and enhances the hydrogel's mechanical properties. LID - E76 [pii] LID - 10.3390/bioengineering6030076 [doi][J]. (2306-5354 (Print)).
- [38] S. Minardi, F. Taraballi, X. Wang, F.J. Cabrera, J.L. Van Eps, A.B. Robbins, M. Sandri, M.R. Moreno, B.K. Weiner, E. Tasciotti, Biomimetic Collagen/elastin Meshes for Ventral Hernia Repair in a Rat model, (1878-7568) (Electronic).
- [39] J. Lee, A.A. Abdeen, X. Tang, T.A. Saif, K.A. Kilian, Matrix Directed Adipogenesis and Neurogenesis of Mesenchymal Stem Cells Derived from Adipose Tissue and Bone marrow, (1878-7568) (Electronic).
- [40] A.S. Mao, J.W. Shin, D.J. Mooney, Effects of substrate stiffness and cell-cell contact on mesenchymal stem cell differentiation, *Biomaterials* 98 (2016) 184–191.
- [41] D.F. Duarte Campos, A. Blaeser, A. Korsten, S. Neuss, J. Jakel, M. Vogt, H. Fischer, The stiffness and structure of three-dimensional printed hydrogels direct the differentiation of mesenchymal stromal cells toward adipogenic and osteogenic lineages, *Tissue Eng. A* 21 (3–4) (2015) 740–756.
- [42] G.J. Her, H.C. Wu, M.H. Chen, M.Y. Chen, S.C. Chang, T.W. Wang, Control of three-dimensional substrate stiffness to manipulate mesenchymal stem cell fate toward neuronal or glial lineages, *Acta Biomater.* 9 (2) (2013) 5170–5180.
- [43] J. Li, N. Tang, May the force be with You, *Dev. Cell* 47 (6) (2018) 673–674.
- [44] Z. Tang, Y. Hu, Z. Wang, K. Jiang, C. Zhan, W.F. Marshall, N. Tang, Mechanical forces program the orientation of cell division during airway tube morphogenesis, *Dev. Cell* 44 (3) (2018) 313–325 e5.
- [45] S.Q. Liu, Q. Tian, J.L. Hedrick, J.H. Po Hui, P.L. Ee, Y.Y. Yang, Biomimetic hydrogels for chondrogenic differentiation of human mesenchymal stem cells to neocartilage, *Biomaterials* 31 (28) (2010) 7298–7307.
- [46] N.J. Hogrebe, K.J. Gooch, Direct influence of culture dimensionality on human mesenchymal stem cell differentiation at various matrix stiffnesses using a fibrous self-assembling peptide hydrogel, *J. Biomed. Mater. Res.* 104 (9) (2016) 2356–2368.
- [47] K. Ye, L. Cao, S. Li, L. Yu, J. Ding, Interplay of matrix stiffness and cell-cell contact in regulating differentiation of stem cells, *ACS Appl. Mater. Interfaces* 8 (34) (2016) 21903–21913.
- [48] J.R. Tse, A.J. Engler, Stiffness gradients mimicking in vivo tissue variation regulate mesenchymal stem cell fate, *PLoS One* 6 (1) (2011) e15978.
- [49] R. Olivares-Navarrete, E.M. Lee, K. Smith, S.L. Hyzy, M. Doroudi, J.K. Williams, K. Gall, B.D. Boyan, Z. Schwartz, Substrate stiffness controls osteoblastic and chondrocytic differentiation of mesenchymal stem cells without exogenous stimuli, *PLoS One* 12 (1) (2017) e0170312.